



Research Article

Development of Recycled Aluminum Alloy for the Manufacture of an Electrical Current-Conducting Tape

Gilson Gilmar Holzschuh^{1*}, Jorge André Ribas Moraes¹, Sérgio Boscato Garcia², Izete Zanescos², Adriano Moehlecke², Rosana de Cassia de Souza Schneider³, Liane Mahlmann Kipper⁴

¹Postgraduate Program in Environmental Technology, University of Santa Cruz do Sul, Santa Cruz do Sul, Brazil

²School of technology, Pontifical Catholic University of Rio Grande do Sul, Porto Alegre, Brazil

³Program in Environmental Technology, University of Santa Cruz do Sul, Santa Cruz do Sul, Brazil

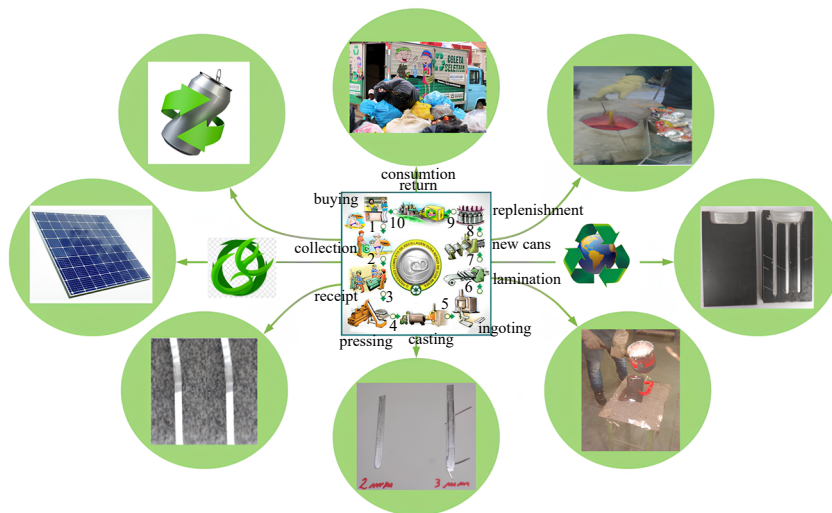
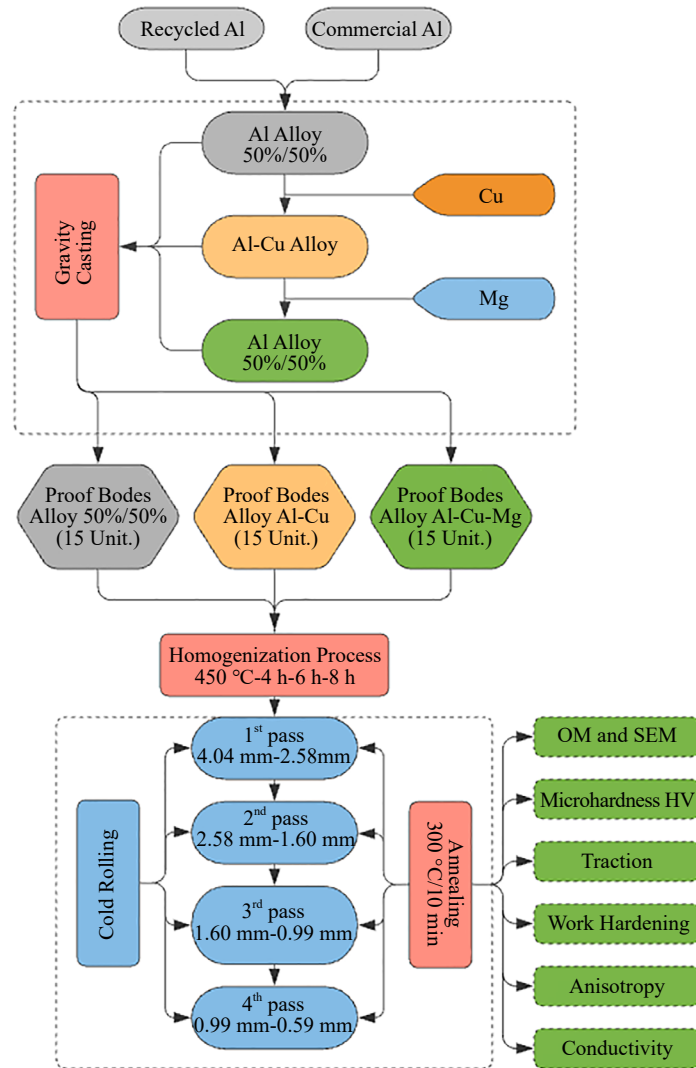
⁴Postgraduate Program in Environmental Technology and Postgraduate Program in Industrial Systems and Processes, University of Santa Cruz do Sul, Santa Cruz do Sul, Brazil

Email: gilsongh@gmail.com

Received: 16 November 2023; **Revised:** 4 March 2024; **Accepted:** 4 March 2024

Abstract: This research aimed to develop an electrical current-conducting tape using secondary aluminum (Al) obtained from recycled beverage cans. The gravity casting process was used, and Cu and Mg were added to assess the properties of the alloys. The evaluated alloys were from three groups of samples: (A) secondary Al; (B) Al-Cu; (C) Al-Cu-Mg. A homogenization process was applied to reduce the segregation of the heterogeneous structure of the cast ingots and to reduce the thickness of the tape to 0.5 mm, the cold rolling process was carried out. The samples were characterized by Vickers microhardness, tensile tests, hardening, anisotropy and electrical conductivity. After four lamination passes a reduction of 85.4% of the initial thickness was observed, reaching (0.59 ± 0.04) mm of final thickness. Subsequently to each lamination pass, the annealing process was applied to restore the material's properties. The electrical conductivity presented results between 45.96 and 47.67 International Annealed Copper Standard (IACS), with a reduction of only 1.82% after lamination. Therefore, a tape with electrical conductivity and 0.59 mm thickness was obtained from recycled beverage cans aluminum. In addition, the characterization presented for the 3 samples will allow for the study of applications for these alloys and respective electrical conductive tapes.

Graphical Abstract



Keywords: recycled aluminum, gravity casting, homogenization, annealing, cold rolling, conductive tape

1. Introduction

Historically copper has been the metal used for the manufacture of electrical conductors, due to its high electrical conductivity for the manufacture of electrical current conductors. However, only 0.01% of the earth's crust contains copper. On the other hand, the aluminum (Al) abundance in the earth's crust is 8.00% and such metal has already good acceptance in the area of electrical engineering, and sold at values well below that of copper [1].

Currently, the installed world power in photovoltaic systems has reached 627 GW [2]. Of this value, approximately 90% of the market is related to modules with solar cells manufactured in crystalline silicon sheets [3] and, in the manufacture of these modules, there is potential for innovations regarding the metals used. The assembly process of the photovoltaic module involves different steps. Firstly, the solar cells are soldered into strips; then these strips are soldered to electrically connect all the solar cells. To complete the manufacture of the standard photovoltaic module, the solar cells are encapsulated as a sandwich, with glass (on the front side) and a polymeric film of ethyl vinyl acetate (EVA) (on the back side). Finally, the module is sealed and the Al structure is used.

A typical solder ribbon used to interconnect the solar cells consists of good conductive material, usually copper, and is covered with a silver alloy that allows to weld the ribbon on the busbar of the solar cell and make electrical, mechanical and thermal contact [4]. Thus, the welding process takes place at temperatures greater than 250 °C and induces thermo-mechanical stresses. Currently, alternative materials and methods are being studied welding crystalline silicon solar cells [5]. The production of primary Al is subdivided into four processes: (i) mining and extraction of bauxite ore, (ii) production of alumina, followed by (iii) smelting the ore and (iv) process of forming the aluminum ingot. In another work, Farajana et al. [6] showed that the primary aluminum casting process has high environmental impacts due to the high consumption of electric power and fuel oil (diesel and natural gas).

A comparative analysis of electricity consumption and greenhouse gas (GHG) emissions was conducted in the primary and secondary aluminum production in China and the United States [7]. The results showed that China's fossil energy consumption and primary Al GHG emissions are double that of the USA. Regarding energy consumption and GHG emissions from the production of recycled Al, compared to the production of primary Al, they are only 6.37% in China and 4.45% in the USA. Maung et al. [8] evaluated secondary Al reserves in 19 countries. They showed that in 2010, 85 million tons of this Al was in the USA, 65 million tons in China, 29 million tons in Japan and 413 million tons in other countries in the world. In the USA, it is estimated that its secondary reserves are larger than its primary reserves and that considerable amounts of secondary Al materials are still accumulated in landfills. A bottleneck in the secondary aluminum reuse process is the formation of slag. According to Mahinroosta and Allahverdi [9], the slag formed in the aluminum smelting process is considered hazardous as industrial waste, posing significant environmental and public health challenges. To reuse this material, both direct and indirect recycling processes can be employed, along with strategies for recovering these residues and methods for managing and reusing these materials.

In this sense, Tsakiridis et al. [10] evaluated the chemical and mineralogical characteristics of the Al salt slag. Formed during the smelting of Al residue, it contains between 15% to 30% Al oxide, 30% to 55% sodium chloride, 15% to 30% chloride potassium, and 5% to 7% metallic Al, as well as impurities such as carbides, nitrides, sulfides and phosphides. Its disposal in landfills is prohibited in most European countries and must be managed in accordance with current legislation. Depending on the crude mixture, the amount of slag can vary from 200 kg to 500 kg per ton of secondary Al throughout the reprocessing activity.

For Capuzzi and Timelli [11], innovations and new trends are related to Al recycling technologies, as well as the evolution of preliminary scrap treatments, such as sorting, crushing and dismemberment. The authors also reviewed foundry technologies, in addition to better operational conditions between costs and efficiency of the casting processes and furnace operation.

The casting process for aluminum cans demonstrates potential since the use of recycled aluminum may reach up to 52% mass [12]. This percentage can be increased to values above 70%, considering the use of a scorifying flow [13]. The chemical analyzes of aluminum alloys showed percentage values above 96% for the element Al. This percentage can be widely explored, aiming to surpass 98%, thus obtaining alloys with higher Al purity contents and, thus,

presenting physical-chemical properties as well as specific mechanical properties.

Innovations and new trends are related to aluminum recycling technologies, as well as, the evolution of preliminary scrap treatments, such as sorting, crushing and dismemberment, also bringing a review of foundry technologies, in addition to demonstrating operational conditions between costs and efficiency of the smelting processes and furnace operation.

Another factor to be considered is the Al smelting processes. These are decisive for the success of secondary Al recycling and reprocessing since the secondary Al alloys are produced from industrial Al scrap and Al waste from recycling. According to Hurtalová et al. [14] these recycled materials contain different alloy elements, such as Al, Cu, Fe, Si and Mg, which form intermetallic phases in the Al matrix and influence the microstructure, basic mechanical properties and interfere with the microhardness of the secondary Al alloy. However, according to Brommer et al. [15], the uncertainty of composition in secondary materials and variable processing conditions inhibit the more significant use of secondary materials in the production of new Al alloys.

One of the challenges for the secondary Al reuse is finding applications that admit in its composition alloys based on secondary Al, resulting in products for commercial use with the same characteristics as those obtained with primary Al. For Ibragimov and Ismailov [16] a solution would be to find alloy elements (solutes) to add to secondary Al-based alloys, which provide the necessary properties of the product of interest. Therefore, Al-based alloys have unique characteristics, among which, are high electrical conductivity, being widely used in energy industries in the production of high-voltage wires.

The use of secondary Al-based alloys involves, on the one hand, the use of traditional steel and Al conductors, with their numerous weaknesses, and on the other hand, design solutions using self-supporting, highly conductive, thermally conductive aluminum alloys and rheologically resistant. An appropriate composition of these elements, as well as the technology of manufacturing and production of alloys (casting, rolling and drawing), creates potential opportunities for obtaining wires and conductors with application properties required by electrical energy engineering [17].

Therefore, the present research aims to develop and analyze secondary aluminum alloys, from the recycling of aluminum cans. Specifically, a secondary aluminum-based alloy was produced and alloy elements were added to enable the best electrical current conduction properties to the alloy formed by the gravity casting process. Lastly, through the cold lamination process, the electrical current conducting tape could be studied as a tape for electrical interconnection of solar cells in the assembly of photovoltaic modules or other applications.

2. Material and methods

Secondary aluminum (beverage cans-that was characterized in [12]), commercial aluminum (6063 T6 alloy), secondary copper (electrical cables) and primary magnesium 99.98% were used in this research. Cu and Mg were used in order to verify the degree of electrical conductivity of the formed alloys, having Al as a base. To fuse the materials, the gravity casting process was used. The molten alloy was drained into a steel mold (chuck) produced specifically for the experiment to form the specimens. The sequence of alloy formation was defined in five steps, as presented in Table 1 [18].

Table 1. Experimental alloy formation sequence

Beatch	Mixture Composition	Temperature Range	
1 st	800 g Al	650 °C	650 °C
2 nd	800 g Al + 30 g Cu	650 °C	650 °C
3 rd	800 g Al + 60 g Cu	650 °C	650 °C
4 th	800 g Al + 60 g Cu + 40 g Mg	650 °C	750 °C
5 th	800 g Al + 60 g Cu + 80 g Mg	650 °C	750 °C

The formed ingot was subjected to the homogenization process aiming at reducing the micro segregations of the structure, conditioning the microstructure in order to improve the workability of the alloy. The homogenized specimens were subjected to the cold rolling process in order to achieve the proposed 0.5 mm thickness. Intermediate annealing was applied among the lamination passes to recover and recrystallize the alloy and so to relieve the mechanical stress and stresses suffered by the material after each accumulated lamination pass. Figure 1 depicts the methodology used in the present research.

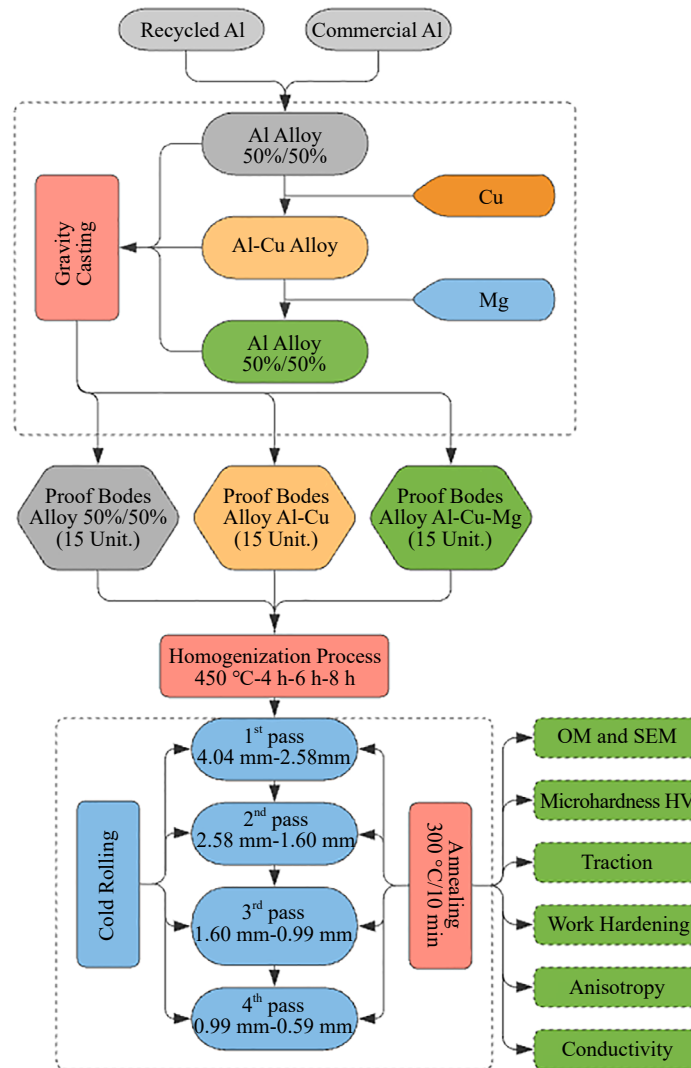


Figure 1. Diagram of the research methodology

2.1 Gravity casting process

For the gravity casting process, an inductive “Well” type oven was used. The oven was preheated until 650 °C, where the metals to be melted were placed. The initial mixing took place using ingots formed in a previous casting process, composed of 50% aluminum from beverage cans and 50% commercial aluminum (alloy 6063 T6) [12]. Table 2 shows the sequence of additions of the alloying elements to the casting process.

Table 2. Casting sequence and alloy formation Al-Cu-Mg

Batch	Composition
samples (A)	Ingot 50% Al cans plus 50% commercial Al
samples (B)	Ingot Al-sample A plus 6% Cu
samples (C)	Ingot Al-sample B plus 8% Mg

In each batch of samples, specimens were formed in triplicate to carry out the subsequent tests. The flow of the melt took place in a mold made with a Society of Automotive Engineers (SAE) (USA) 1045 steel plate, 300 mm long and 100 mm wide. The three channels were dimensioned with 2 mm, 3 mm and 4 mm of depth. For the exit and escape of gases, small oblique cuts were made on the sides of the shell and connected to the specimens, and vertical cuts at the base of the specimens for the directional exit of the gases at the bottom of the three channels, as shown in Figure 2.

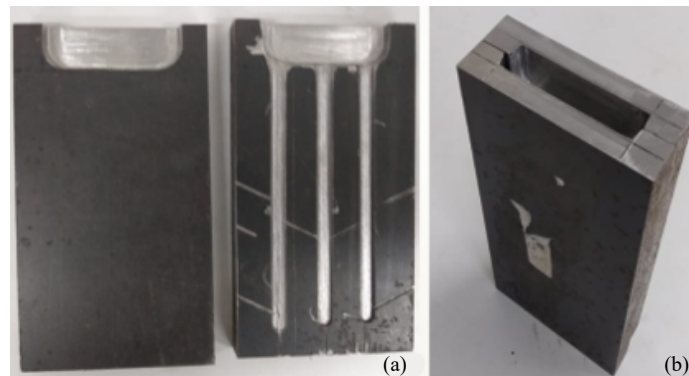


Figure 2. Views of the chill mold. (a) Chill partitioned with the flow channels in detail. (b) Top view of the shell assembled to receive the melt

Aiming to avoid the spillage during the flows, a cavity was made in the upper part of the two pieces of the chill mold, and so direct the material to the main channels. In this cavity, a rectangular specimen was formed after the material cooling. This specimen was used as a sample to perform chemical analysis, micrography, traction and hardness for validation of the mixture and verification of properties at each stage of the experiment.

In order to obtain a homogeneous flow of the melt in the mold, and a non-accelerated cooling of the melt, the mold was heated in a muffle furnace, keeping it constant at 450 °C. The mold was removed from the oven to drain the specimens. Then, again inserted in the oven to return the temperature predicted for the next flow. Due to the addition of magnesium, an injection of argon gas was used on the bath surface to control the solubility of magnesium in contact with oxygen [19].

2.2 Preparation and heat treatment of the samples

The samples were submitted to the homogenization process aiming at the redistribution of the elements within the alloy structure and to minimize micro-segregation, resulting in a conditioning treatment of the microstructure, and, in this way, increasing the alloy workability [20]. Then, the lamination process was applied in order to reduce the thickness of the material, to reach a thickness of 0.5 mm. Based on Engler [21] after each lamination pass, an annealing process was carried out in order to recover the properties of the deformed material, eliminating discrepancies and later recrystallization through the formation of new smaller, equiaxial grains and concentration of crystalline defects inferior to the hardened state.

2.3 Homogenization

In order to monitor the evolution of the intermetallic phases in the abnormal growth of the grains, the samples were submitted to a homogenization process for 8 h at 450 °C. Cooling was carried out inside the oven for 24 h and the samples were removed with thermal equilibrium at room temperature. After 4, 6 and 8 h carrying out the process, samples were taken for analysis, and micrography was performed.

2.4 Annealing

After cold deformation, the specimens were annealed to recover the crystalline structure of the metal, decrease the mechanical strength and increase the ductility of the material. According to Mankins [22] during the annealing occur recovery, recrystallization and grain growth.

The concurrent existence of phenomena, such as the partial elimination of discrepancies resulting from the movement of linear defects through slip and jump mechanisms, may facilitate the detection of discrepancies with opposite signs that mutually nullify each other [23]. In this process, the internal energy was reduced in part, still small, and the internal stresses were relieved substantially, facilitating the subsequent lamination processes. Based on Tajally et al. [24] the samples were inserted in the muffle furnace for 10 minutes at 300 °C after the oven stabilization. After 10 min, the samples were removed from the oven and cooled to room temperature. The process was repeated, thereupon each pass in the cold rolling process, until reaching the final thickness of 0.5 mm.

2.5 Cold rolling

After homogenization, the specimens were cold rolled to reduce the final thickness to 0.5 mm. The reduction applied to the specimen in each pass was 38%, where the initial thickness was 4 mm. The specimens, after each pass in the laminator, were subjected to the annealing process to recrystallize and recover the mechanical properties, relieving the stress and tensions suffered in the lamination process. A bench laminator with a 10 times reduction capacity, able to receive materials with a thickness of up to 5 mm and a minimum outlet thickness of 0.5 mm was used. The laminator owns four pass routes, with approximately a 40% reduction in each pass. Based on the initial measurement of the samples (4 mm), the 40% reduction capacity in each lamination pass and the final thickness (target 0.5 mm), four passes were performed. The thickness measurements after each pass were recorded and statistically evaluated.

2.6 Metallographic preparation

The samples were cut in the lamination direction. For grinding, grenades of SiC 220, 400 and 600 mesh were used. For the initial polishing of the samples, 4.0 µm diamond paste and ethylene glycol lubricant were used for 20 min. In the intermediate polishing, 5.0 mg of powdered MgO diluted in 30 mL of distilled water for 3 min was used as an abrasive. To reveal the microstructure, an electrochemical attack was used with a solution of 5.4% hydrofluoric acid in 94.6% distilled water, 1.5 A of electrical current and 20 V for 3 minutes at room temperature. The equipment used was a hot source of direct current and a magnetic stirrer. The solution was kept under stirring and a commercially pure aluminum disk was used as a cathode.

2.7 Chemical analysis

After each batch (Table 2), samples were taken according to American Society for Testing and Materials (ASTM) E716-98, to perform the chemical analysis and identify the composition resulting from the mixture proposed in the experiment. These analyses were performed by the optical emission spectroscopy technique, using an optical spectrometer, according to ASTM E1251-99.

2.8 Microstructural analysis

Sample thicknesses were obtained by polarized light microscopy (PLM). The microstructural characterization of the samples was carried out using a scanning electron microscope (SEM) with secondary electron detectors (SED)

and an X-ray analyzer, Phillips model Filament emission field (FEG)-Inspect 50. Dispersive spectroscopy was used to determine the presence of secondary phases and to measure the composition of the grains in different positions. The volumetric fraction of the secondary phases at the grain limit was evaluated using a quantitative X-ray wavelength dispersive spectroscopy (WDS) system attached to the Electron probe microanalysis (EPMA) instrument (Microanalysis by Electronic Probe) performed on an Electron Probe JXA-8230 Microanalyzer operating at 20 kV.

2.9 Vickers microhardness test

After metallographic preparation, microhardness measurements were carried out with a load of 0.5 kg for 15 s in a microdurometer Zwick model 3212 B [23]. Random measurements were made along the sample surface in each test. The final value resulted in the average obtained by the number of tests applied to each sample.

2.10 Tensile test

For the tensile tests, three samples of rectangular sections were collected in each of the following directions: 0°, 45° and 90°, in the different thicknesses of the material, with the direction of lamination as a reference. For finishing, a vertical band saw, cutter and a file were used. To check the thickness, a Mitutoyo micrometer was used while for elongation measurement, a 25 mm extensometer was used. In the testing machine (PIW ZD 10/90), a 200 kg load cell was used (Kratos KM model). The tests followed the Standard Test Methods of Tension Testing Wrought and Cast aluminum and magnesium-Alloy Products ASTM B 557-02.

2.11 Determination of hardening and anisotropy coefficients

To verify the hardening properties, based on the stress versus strain graph, the uniaxial stress test was used. According to Ghosh et al. [25] to determine the hardening coefficients n and R of Lankford, samples of the materials were taken in the 0°, 45° and 90° directions in the lamination direction. A digital caliper and a digital micrometer with a spherical tip were used to measure the thickness and width of the specimens before and after each lamination pass. The calculation of the n value was performed according to the standard ASTM E646-00 (Standard Test Method for Tensile Strain-Hardening Exponents (n-Values) of Metallic Sheet Materials). The normal and planar anisotropy coefficients were obtained through tensile tests, according to the standard ASTM E517-00 (Standard Test Methods for Plastic Strain Ratio r for Sheet Metal).

2.12 Electrical conductivity tests

The electrical conductivity was measured using a digital contact conductive meter, model Tecatron DC-9. The conductivity calibration was performed with an aluminum standard (in 58.2 IACS at 20 °C). The measurements given are percentages of the conductivity of annealed copper according to the International Annealed Copper Standard (IACS). Thus, a material with 58.2 IACS corresponds to 58.2% of the standard copper conductivity. For each formed alloy, three specimens were used and, in each sample, five measurements were made. For the conductivity result, the average of the three samples with five measurements was considered whereas for the degree of dispersion of the data in relation to the average, the standard deviation was applied.

3. Results and discussion

The samples previously defined in Table 2 showed the results of the chemical analysis according to Table 3. The percentages of Al reduced proportionally in relation to the addition of Cu and Mg. Sample (A) was considered as the base, and 6% Cu was added to form sample B. Since Cu has a higher melting point (1,083 °C) in relation to Al, the melting temperature was increased from 650 °C to 780 °C, which justifies the difference in the reduction of Al (10.04%), by the increase of 7.89% of Cu, being then 2.15% of Al dissolved.

Table 3. Chemical analysis of the Al alloy

Samples	Elements (%)								
	Al	Mg	Mn	Fe	Cu	Si	Zn	Cr	Ti
(A)	98.20	0.78	0.30	0.28	0.10	0.24	0.03	0.02	0.00
(B)	88.16	0.63	0.34	0.38	7.89	0.63	1.85	0.01	0.02
(C)	82.79	6.77	0.37	0.38	7.00	0.56	1.96	0.01	0.02

For the sample formation (C) only 8% Mg was added over the melt from the previous step. In this step, the initial temperature of 650 °C was returned since Mg was easily fused by the diffusion process. Thus, the percentage of Al reduction (5.37%) was close to Mg (6.77%) added.

Cu was 1% above and Mg was 1.2% below the planned percentage for the experiment. This is because Mg has a high affinity for oxygen in the molten state and, unlike other metals, it does not form a stable protective film on the surface of the molten products. Even with the use of a controlled atmosphere in argon, Mg dissolved, explaining its percentage reduction as shown in Table 3 [26].

3.1 Structure and composition of the alloy

To characterize the microstructure of the alloys (A), (B) and (C), formed by the gravity casting process, Optical Microscopy (OM) analysis was performed. As can be visualized in (Figure 3 (A), (B) and (C)), a eutectic structure exhibiting severe dendritic segregation, consisting of two intermetallic phases was formed.

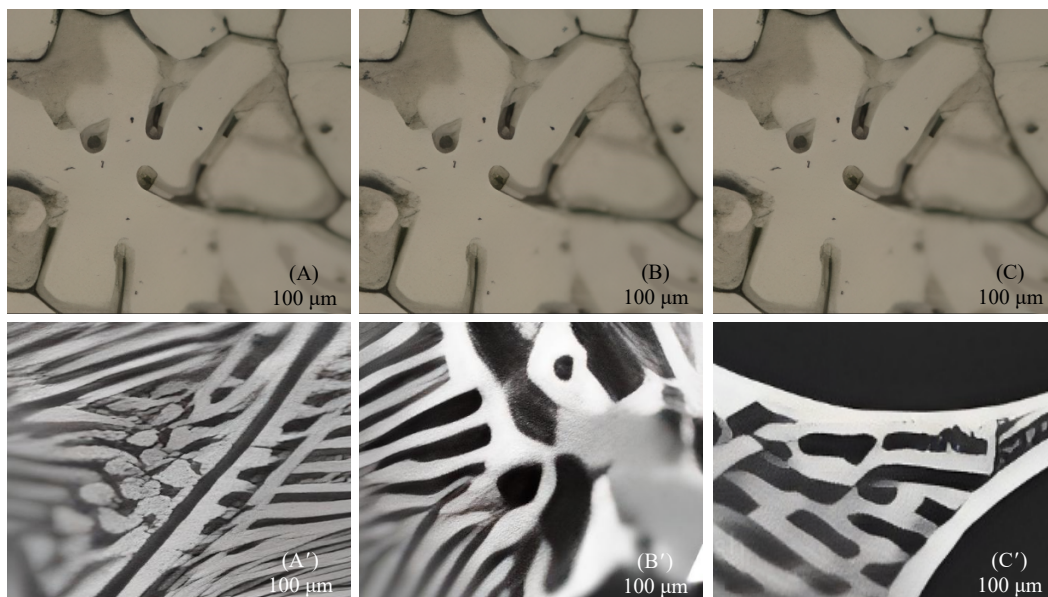


Figure 3. Analysis MO and WDS of the samples before lamination. Figure 3 (A), (B) and (C) shows analysis of SEM at 100 μm. Figure 3 (A'), (B') and (C') shows the quantitative analyzes of the WDS

The analyzes in WDS present an atomic composition of the white intermetallic phase between 18.72-21.01% of Cu, 24.20-27.71% of Mg, 3.48-4.01% of Zn and a balance in Al close to the S phase (Al_2CuMg), however, with Cu content below the S phase [27-29]. Likewise, the atomic composition of the gray intermetallic phase is between 24.11-26.72% of Cu, 3.91-4.24% of Mg, 0.60-0.66% of Zn and the balance in Al close to because the Cu content is lower than

the θ phase. In addition, the white intermetallic phase dissolves small amounts of Zn and the gray intermetallic phase dissolves small amounts of Mg.

Similar results were found by [27]. In your research, particles associated with the phase such as $MgZn_2$ are dissolved after remaining for 5 minutes in the annealing process at 475 °C. On the other hand, particles associated with the S phase such as Al_2 and $CuMg$ exhibit a comparatively higher resistance to dissolution. Achieving their complete dissolution necessitates a stepwise solution treatment [27]. Likewise [30] dissolved Zn atoms in the matrix with temperatures close to 430 °C where the transition zone between the η to S phases occurs. The Cu element showed a diffusion rate at 450 °C in the S phase (Al_2CuMg), while Mg at 460 °C.

3.2 Homogenization

The microstructure after homogenization is represented by Figure 4. As can be observed, the microstructure of the samples showed the evolution of the intermetallics during the homogenization process. After treatment at 450 °C and after the first 4 h of homogenization, large intermetallic phases without equilibrium are distributed along the grain boundaries, as represented by Figures 4 (A), (B) and (C) at 100 μm .

The volumetric fraction of the residual phases and of the dendritic network structure are significantly reduced after the second and third stages of homogenization. At the same time, the grain boundaries become thinner. Furthermore, it was verified that prolonging the homogenization time of the third step, did not lead to a distinct alteration of the microstructure in the optical analysis, and the phenomenon of excessive burning was not observed.

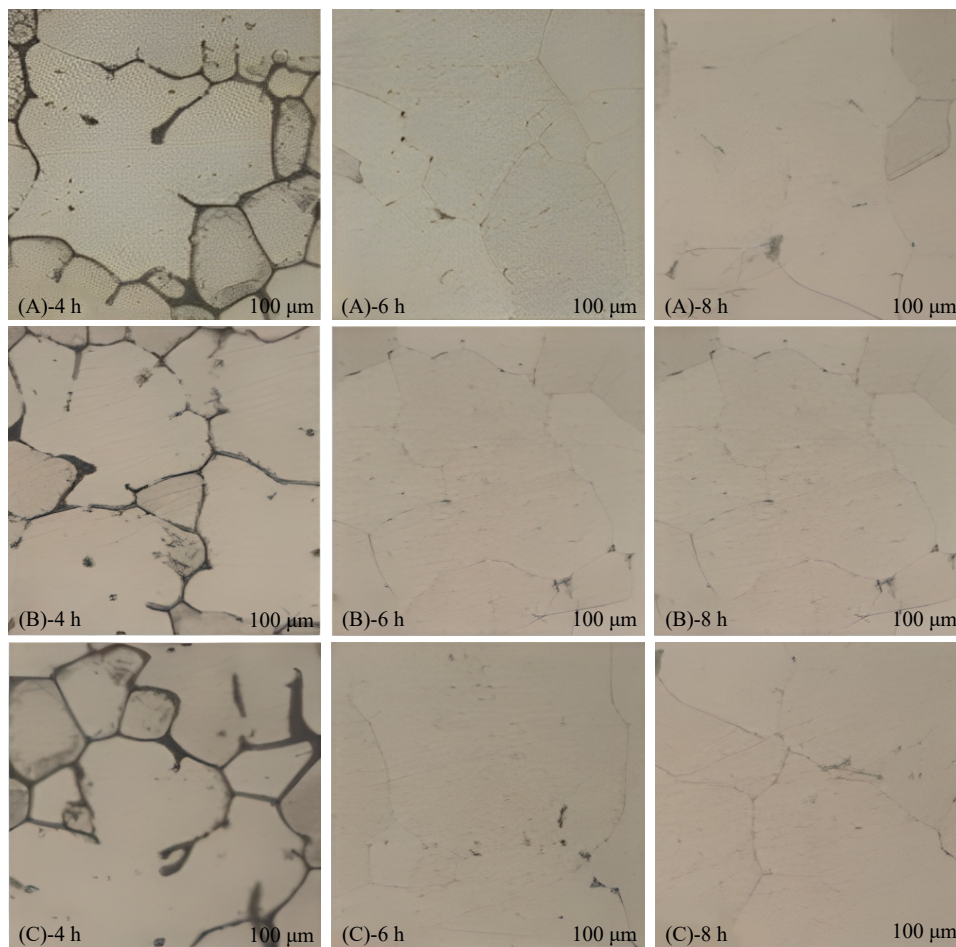


Figure 4. Microstructure after the homogenization process of the samples (A), (B) and (C) taken after 4 h, 6 h and 8 h at 100 μm

3.3 Lamination process

With the homogenized specimens, the lamination process was carried out. The mean data of input and output of the process, as well as the standard deviation and reduction percentage of thickness at the end of each lamination pass, are presented in Table 4.

Table 4. Lamination measurements (mm) and reduction percentage of thickness

Lamination order	Input (mm)	Output (mm)	Standard deviation (mm)	Reduction (%)
1 st pass	4.04	2.58	0.081	36.10
2 nd pass	2.58	1.60	0.077	38.00
3 rd pass	1.60	0.99	0.080	38.10
4 th pass	0.99	0.59	0.075	40.40

The thickness reduction occurred regularly within the same group of samples. The specimens of the group (A) better supported the reduction of each pass, presenting linear deformations in the rolling direction and few fractures in the specimens. However, the specimens of groups (B) and (C), showed curvatures in transversal directions in some samples, revealing fractures, including complete ruptures. This behavior may be ascribed to the percentage aggressiveness of the pass (40%), which, in turn, may be related to the level of hardness of the alloy, when adding Cu and Mg, as well as the increase of the mechanical resistance and reduction of the ductility. To reduce these effects, the annealing process was applied after each lamination pass.

3.4 Annealing

As the purpose of the lamination process was to reduce the thickness of the specimens from 4 mm to 0.5 mm, the annealing heat treatment was applied. In this treatment, recovery and recrystallization processes take place aiming to restore the mechanical properties, relieve tensions and reduce the energy stored by the movement of discrepancies. In addition, the annealing allows for the reorganization of the crystals of the material structure. Figure 5 shows the PLM images with a 50-fold magnification.

PLM images indicated a grain structure with elongated contours in the lamination direction. The precipitates present in the material may explain the non-linearity of the contours, promoting their support and, thus, making their migration difficult during recrystallization. This morphology indicates that the growth rate of recrystallized grains is higher in the lamination direction than in the transversal direction, possibly due to the alignment of the second phase particles in the lamination direction.

The colors related to the spatial or crystallographic orientation of each grain are poorly defined for some grains, indicating possible regions with sub-grains that have not yet migrated during recrystallization, being responsible for color defects. These phenomena occur due to partial recrystallizations, as it is expected with a completed recrystallization, a structure of equiaxial grains and well-defined contours. Similar grain structures were found by Goloborodko et al. [31].

Thus, possible deformations in the specimens of samples (B) and (C) occurred during the lamination process due to the fact that there are still crystalline defects not completely eliminated by the recovery and recrystallization process, indicating the need for annealing times greater than 10 minutes, as defined by the methodology.

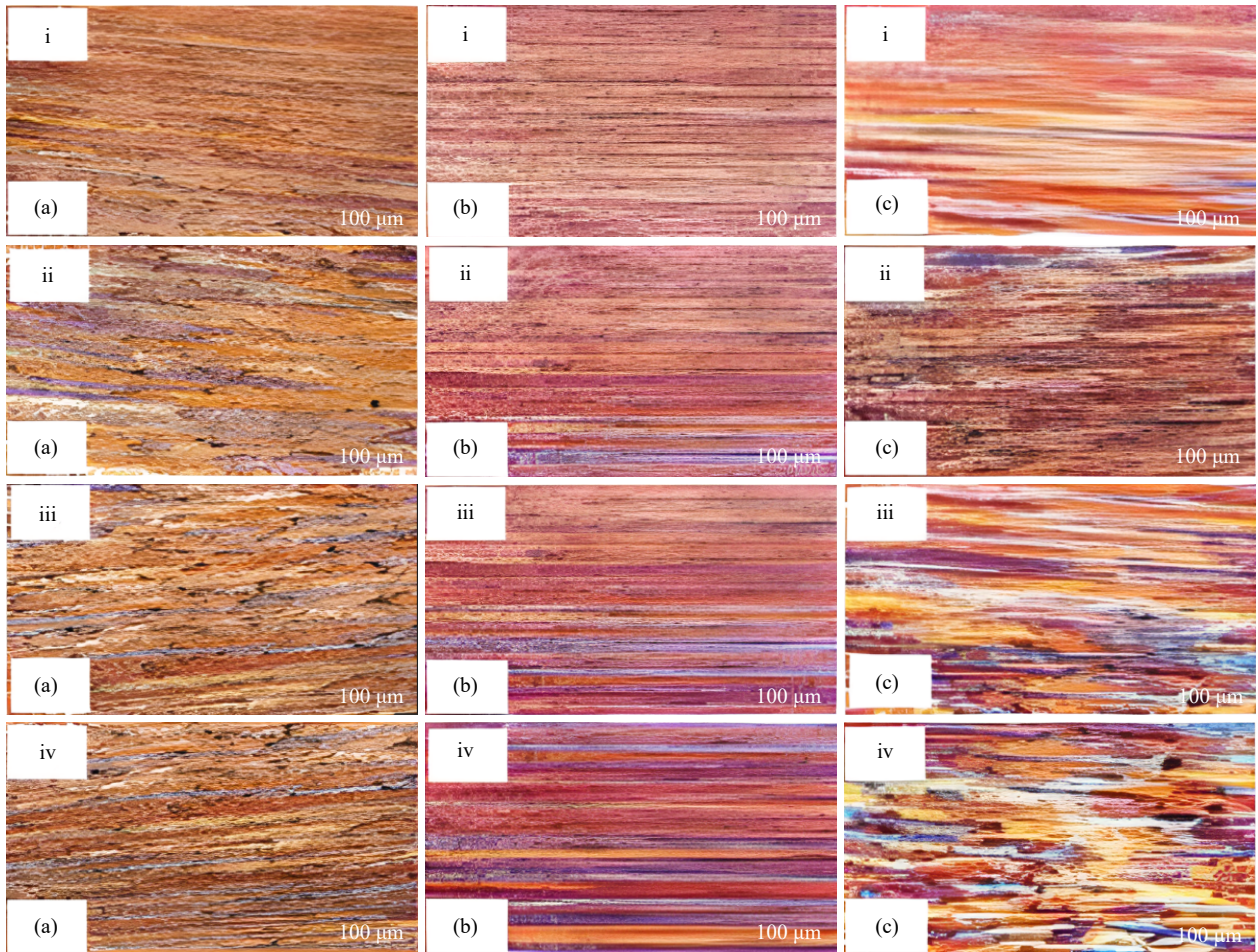


Figure 5. PLM images of the lamination direction throughout the annealing process. Where (a), (b) and (c) represent the samples and i, ii, iii and iv represent the annealing sequence after each lamination pass

3.5 Vickers microhardness

The Vickers microhardness tests were applied after the completion of each lamination pass and the respective annealing heat treatment. Their goal was to assess the level of hardening and its effect on the annealing process on the laminated samples. In Table 5, the first line presents the microhardness values found for the samples (A, B and C), being the average of each sample before lamination, only fused and homogenized.

Table 5. Evolution of microhardness in relation to the reduction in the lamination process percentage

Lamination order	Thickness (mm)	Redution (%)	Microhardness (HV)		
			Sample A	Sample B	Sample C
Molten	4.04	0.00	68	72	78
1 st pass	2.58	36.14	84	90	97
2 nd pass	1.60	60.40	106	112	122
3 rd pass	0.99	75.50	132	140	152
4 th pass	0.59	85.40	166	175	190

In Table 5, the average microhardness of the samples is represented after each rolling stage and subsequent annealing. Finally, at the end of the 4th rolling and annealing pass, the general average and standard deviation of the materials analyzed in the research were represented. It was observed that during the cold rolling process, and the consequent increase in hardening of the samples, the microhardness increased gradually and linearly, as the thickness was reduced. When analyzing the general averages of the three samples, it was found that the addition of Cu (B) on the aluminum base (A), increased the microhardness by 6.07%, as well as the addition of Cu and Mg (C) in relation to the aluminum base (A), increased microhardness by 14.9%. When compared to the addition of Mg over the Al + Cu (B) alloy, the microhardness was increased by 8.39%. The highest microhardness results of the samples occurred at the end of the 4th lamination pass. At this condition, samples (C) presented a microhardness of 190.34 HV, representing values 8.28% and 14.65% higher than the maximum averages presented by (B) and (A), respectively.

The sample's behavior along the deformation process might be related to the efficiency of the recrystallization process performed on the samples before each applied deformation. This characteristic can also be visualized in Figure 6, where the symmetry and dispersion of the samples are depicted.

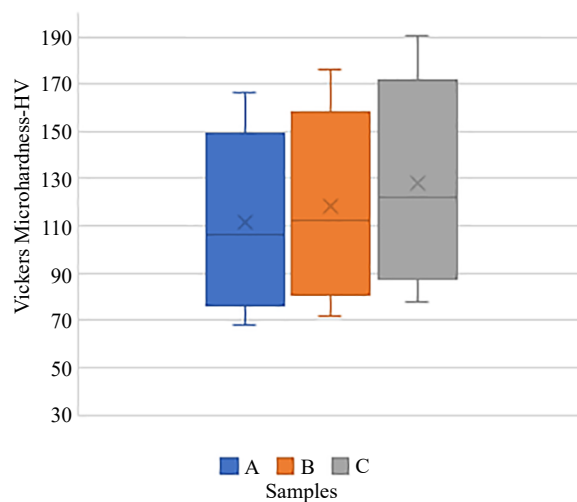


Figure 6. Symmetry and dispersion of the samples cold laminate

It was verified that the microhardness increases with the thickness decreases through the lamination process. To confirm the data presented in Table 5, the Spearman correlation coefficient was applied, which is a non-parametric coefficient, due to the small sample, following the recommendations of [32].

The result confirmed the linearity of the samples with the Spearman correlation coefficient, where the value found (-1) indicates a perfect negative linear relationship. Likewise, the Spearman correlation coefficient = 1, indicates a perfect positive linear relationship, with ($p < 0.05$) and all significant samples. To corroborate these results, the Kruskal-Wallis non-parametric test was applied, where again $p = 0.011 < 0.05$, indicating that there are no significant differences between the medians of samples A, B and C.

3.6 Tensile tests

The performance of the tensile tests aimed to obtain information about the mechanical properties of the specimens after the suffered deformation. Figure 7 shows the tensile tests in the lamination direction with variations of 0°, 45° and 90°.

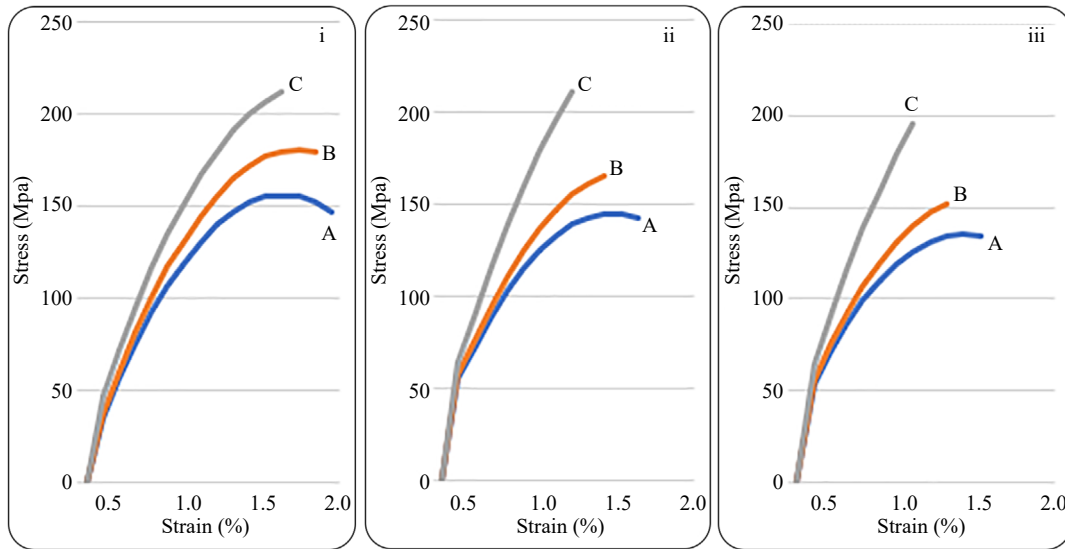


Figure 7. Stress-strain curves after each rolling pass. i) 0° in the lamination direction, ii) 45° in the lamination direction, iii) 90° in the lamination direction. (A)-Blue color, (B)-Orange color and (C)-Gray color

The obtained results showed that with the increase of the material cold deformation, the limits of flow and resistance decrease, highlighting the typical curves of fragile materials. On the one hand, the behavior of samples (C), in relation to 0°, 45° and 90°, showed superior limits of tensile strength in relation to samples (A) and (B). On the other hand, they broke with 1.25% deformation at 0°, and 1% at 45° and 90°, and samples (A) broke at 1.7% at 0° and 1, 65% at 45° and 90°; and samples (B) broke by 1.5% at 0° and 1.25% at 45° and 90°. Thus, the early rupture of samples (C) and (B) is attributed to the addition of Cu and Mg on the aluminum base (A) and higher values in terms of hardness, as shown in Table 4.

Figure 7 shows a very small plastic region and early ruptures at low deformations, characteristics of significantly fragile materials. In this respect, the deformations presented by the specimens during the lamination process are justified, where fractures were noticed at the edges of the specimens in the form of cracks and inside cracks. In addition, the deformation caused by the lamination process, 85.4% of the final thickness in relation to the initial one, resulted in an elongation of the grain in the lamination direction. It was observed that arrangements of discrepancies in the material cause such ruptures, not allowing the deformation to continue and increasing the stacking fault energy (SFE) [33]. To corroborate these arguments, an analysis of the level of hardening and anisotropy of the material was carried out.

3.7 Coefficients of hardening and anisotropy

The tensile tests, in addition to producing values for yield limits, limits of tensile strength, and percentage elongations, were fundamental to obtain the hardening level and anisotropy rates represented by Table 6 [34-36].

Considering the average hardening level (η mean) of each sample, the average resulting from the three samples, was in the range of 0.165, with a standard deviation around 0.0465 indicating a high level of hardening at the end of the lamination. This is reflected by the low ductility of the material, which can also be verified in Figure 7. As can be seen, the samples have a plastic region with small elongations. In addition, it presents similar yield and tensile strength limits, including values very close to the material's string point. This characteristic is more exposed in samples (B) and (C), demonstrating a severe fragility of the same.

Moreover, there is also a high need to force application to the material for flow and small deformations in order to 1.0 to 1.7%, meaning that the material presents a very restricted plastic region, with flows occurring close to the rupture of the material.

However, the normal anisotropy index resulted in relatively high values, at a level of 0.78, indicating a tendency for the material not to resist to the deformation applied by the lamination process. Negative values of planar anisotropy (ΔR) indicate that the material easily presents the formation of earing (folds) in the direction of 45° of the lamination,

not occurring in the directions 0° and 90° .

Table 6. Hardening Values of the exponent η and the anisotropy index R , \bar{R} and ΔR in the respective lamination directions

-	Position	Sample A	Sample B	Sample C
R	R_0	0.778	0.784	0.791
	R_{45}	0.767	0.771	0.776
	R_{90}	0.748	0.753	0.759
Standard Deviation	-	0.015	0.016	0.016
\bar{R}	-	0.765	0.770	0.776
ΔR	-	-0.004	-0.003	-0.001
η	R_0	0.216	0.204	0.199
	R_{45}	0.193	0.172	0.158
	R_{90}	0.123	0.112	0.109
Standard Deviation	-	0.048	0.047	0.045
$\eta_{average}$	-	0.177	0.163	0.155

3.8 Electrical conductivity

The first analysis of electrical conductivity was performed with homogenized specimens. The analysis aimed at reducing precipitates, as well as the solid solution of elements containing Fe and Mn, which provide for the reduction of electrical conductivity. This stage, preliminary to the lamination process, presented the highest measurements of electrical conductivity in relation to the samples, later laminated. As shown in Figure 8, with the application of four lamination passes, a reduction in electrical conductivity occurred.

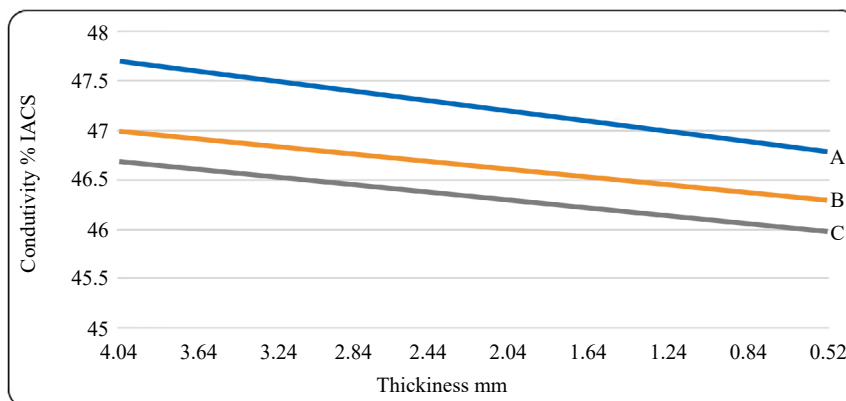


Figure 8. Electrical conductivity of the samples in IACS

Nevertheless, the reduction in electrical conductivity did not occur in the same proportion as for the thickness. While the thickness reductions reached values of 85.4% the electrical conductivity decreased by 1.82, 1.62 and 1.52% to samples A, B and C, respectively. A higher reduction in conductivity was expected because the cold rolling process

tends to increase the number of discrepancies, which implies decreasing the ductility of the material, increasing the hardness and consequently reducing the electrical conductivity [37-38].

To reduce these aggressive effects of lamination on the specimens, the annealing heat treatment was applied, providing a restoration of the material's properties, and confirming the lower reduction in electrical conductivity.

3.9 Future perspectives

This material has an appropriate physical profile to produce tapes to be used in solar cells. Nevertheless, the results of preliminary tests showed that the weldability of these tapes in the cells was not efficient. Therefore, there is a need to add specific materials to improve the welding properties of the produced alloy, adding elements in the casting process or performing superficial bathing processes on the finished tape, where this outer layer is responsible for welding the tape and, the inner layer, for the conduction of electric current.

In order to encourage the use of recycled aluminum, it is also possible to design the secondary aluminum-based alloy as a metallic structure that shapes the Photovoltaic Module. For this application, there will be no need to analyze the conductivity of the material, since it will not have such a function, only considering physical and mechanical properties such as impact resistance, hardness, deformation and corrosion resistance.

For other applications or even to further improve the ability to conduct electricity, it is recommended to carry out studies with recycled aluminum using as reference 6xxx series alloys, such as alloy 6101, used in the manufacture of electrical conductors and overhead cables in electrical networks performed mainly by Karabay and others authors [1, 39-44]. Additionally, using refiners such as AlB_2 to eliminate intermetallic that reduce electrical conductivity, as well as performing the lamination process with less aggressive reductions in each pass, to avoid excessive hardening and other effects.

4. Conclusions

The gravity casting process proved to be efficient for the formation of recycled aluminum alloy from cans. The best drainage results occurred due to the temperature of the 450 °C of the mold and due to the removal of the oven when draining.

Regarding the alloy characterization, two intermetallic phases were detected by optical microscopy, S (Al_2CuMg) and θ (Al_2Cu) and indicated dissolution of Zn and Mg. These results were considered for the application of the homogenization process, where a reduction in the volumetric phase was observed, including the intermetallic phases, besides indicating the dendritic network reduction and the formation of finer grain boundaries.

The lamination process proved to be aggressive in terms of reduction parameters. Although the 38% reduction is excessive for a single pass, a thickness of 0.5 mm has been achieved. The samples in group (A), withstood the successive rolling passes more easily, compared to the samples in groups (B) and (C) that suffered rupture and fractures that were attributed to the presence of Cu and Mg and contamination with Zn.

From the Vickers microhardness analysis, it was found that the samples produced are fragile, with little ductility, presenting a small plastic region, with tightness occurring just after the tensile strength limit point. The microhardness showed maximum values for the samples (C), 190.34 HV. The addition of Cu in the aluminum-based alloy implied an increase of 6.07%, and over Al-Cu, the addition of Mg (C) increased by 8.28% compared to the Al-Cu (B), as well as 14.65% on the Al (A) based alloy.

The tensile tests also evaluated the lamination process in three directions: 0°, 45° and 90°, in which the 0° direction presented superior plastic regions and the 90° direction suffered less deformations. In general, the average hardening level of 0.16, which is close to 0, and the normal anisotropy of 0.77, close to 1, indicate the tendency of the material to present little resistance to undergo deformations, and may suffer tightness very close to the limit of tensile strength. The negative (planar anisotropy) indicates the tendency to form ears and folds in the 45° direction.

The analysis of electrical conductivity showed that the material can be used as a conductor, with effects of falling conductivity associated with the results of traction and hardness and the increase of discrepancies in the grain contours. The samples before lamination showed electrical conductivity between 46.75 and 47.75 IACS and after the application of 85.4% thickness reduction, the conductivity reduced only 1.82%. This result is ascribed to the annealing process

carried out after the application of each lamination pass.

In this way, we completed the objective of building an electrical current conductive tape composed of 50% aluminum obtained from recycled beverage cans and 50% commercial aluminum, secondary copper obtained from recycled electrical wires and primary magnesium 99.85% pure, as specified in the methodology.

Acknowledgments

National Research Council (CNPq) process 310228/2019-0 and 303934/2019-0.

Statement of originality

We hereby declare that this submission is our own work and to the best of our knowledge it contains no materials previously published or written by another person.

CRedit authorship contribution statement

*Gilson Gilmar Holzschuh: Conceptualization, Methodology, Validation, Writing-original draft, Visualization, Formal analysis, Investigation. Jorge André Ribas Moraes: Supervision, Validation, Writing-review & editing. Sergio Boscato Garcia: Validation, Writing-review & editing. Izete Zanesco: Validation, Writing-review & editing. Adriano Moehlecke: Validation, Writing-review & editing. Liane Malmann Kipper: Validation, Writing-review & editing. Rosana de Cássia Schneider: Validation, Writing-review & editing.

Data availability

The raw/processed data required to reproduce these findings cannot be shared at this time as the data also forms part of an ongoing study.

Conflict of interest

The authors declare that they have no known competing financial interests or personal relationships that could have appeared to influence the work reported in this paper.

This study was funded in part by the National Research Council (CNPq) process no 310228/2019-0 regarding the productivity grant granted to researcher Rosana C. S. Schneider, and by process no 303934/2019-0 regarding the productivity grant granted by the National Research Council (CNPq) to researcher Liane M. Kipper.

References

- [1] Karabay S, Uzman I. Inoculation of transition elements by addition of AlB_2 and AlB_{12} to decrease detrimental effect on the conductivity of 99.6% aluminium in CCL for manufacturing of conductor. *Journal of Materials Processing Technology*. 2005; 160(2): 174-182.
- [2] Brunisholz MJ. Instantâneo dos mercados fotovoltaicos globais. Available from: <http://www.ica-pvps.org> [Accessed 20 May 2020].
- [3] ITRPV. International technology roadmap for photovoltaic. Available from: <https://itrpv.vdma.org/> [Accessed 20 May 2020].
- [4] Zarmai MT, Ekere NN, Oduoza CF, Amalu EH. A review of interconnection technologies for improved crystalline

- silicon solar cell photovoltaic module assembly. *Applied Energy*. 2015; 154: 173-182.
- [5] Guo W, Ma X, Gao M, Yan J. Direct soldering of screen-printed Al-paste layer on back-side of silicon solar cell using SnAg solder. *Materials Letters*. 2018; 231: 146-149.
 - [6] Farjana SH, Huda N, Mahmud MAP. Impacts of aluminum production: A cradle to gate investigation using life-cycle assessment. *Science of the Total Environment*. 2019; 663: 958-970.
 - [7] Beeley P. *Foundry Technology (Second Edition)*. Oxford: Butterworth-Heinemann; 2001. p. 687-698.
 - [8] Maung KN, Yoshida T, Liu G, Lwin CM, Muller DB, Hashimoto S. Assessment of secondary aluminum reserves of nations. *Resources, Conservation and Recycling*. 2017; 126: 34-41.
 - [9] Mahinroosta M, Allahverdi A. Hazardous aluminum dross characterization and recycling strategies: A critical review. *Journal of Environmental Management*. 2018; 223: 452-468.
 - [10] Tsakiridis PE. Aluminium salt slag characterization and utilization: A review. *Journal of Hazardous Materials*. 2012; 217: 1-10.
 - [11] Capuzzi S, Timelli S. Preparation and melting of scrap in aluminum recycling: A review. *Metals*. 2018; 8(4): 249.
 - [12] Holzschuh GG, Dörr DS, Moraes JAR, Garcia SB. Metal matrix production: Casting of recycled aluminum cans and incorporation of rice husk ash and magnesium. *Journal of Composite Materials*. 2020; 54(22): 3229-3241.
 - [13] Verran GO, Kurzawa U. An experimental study of aluminum can recycling using fusion in induction furnace. *Resources, Conservation and Recycling*. 2008; 52(5): 731-736.
 - [14] Hurtalová L, Tillová E, Chalupová M. Microstructural and Vickers microhardness evolution of heat treated secondary aluminium cast alloy. *Key Engineering Materials*. 2014; 586: 137-140.
 - [15] Brommer T, Olivetti E, Gihleengen BE, Riddervold HO, Øyen G, Kirchain R. Increased recycled aluminum content during remelting by incorporating compositional uncertainty. *EPD Congress 2011-TMS 2011 Annual Meeting and Exhibition*. San Diego, CA; 2011. p. 939-946.
 - [16] Ibragimov X, Ismailov N. Development of lean titanium-alloyed aluminium alloy for electro-technical purposes. *Eastern-European Journal of Enterprise Technologie*. 2018; 1(12): 23-29.
 - [17] Smyrak B, Knych T, Mamala A, Uliasz P, Jabłoński M. A study of a new generation of multi-functional aluminium alloys for the power industry. *Key Engineering Materials*. 2011; 641: 439-442.
 - [18] Holzschuh GG, Moraes JAR, Garcia SB, Zanesco I, Kipper LM. Casting of recycled aluminum cans to electrical conductivity tape production. *Journal of Waste Management & Recycling Technology*. 2023; 1(2): 1-7.
 - [19] Achyuth K, Patel M, Sangral S, Jayaprakash M. Fretting wear degradation behavior of Al-Si-Ni based cast Aluminum alloy under different environment. *Materials Today: Proceedings*. 2019; 15: 103-108.
 - [20] Pedersen KO, Westermann I, Furu T, Børvik T, Hopperstad OS. Influence of microstructure on work-hardening and ductile fracture of aluminium alloys. *Materials and Design*. 2015; 70: 31-44.
 - [21] Engler O. Texture and anisotropy in the Al-Mg alloy AA 5005-Part I: Texture evolution during rolling and recrystallization. *Materials Science and Engineering: A*. 2014; 618: 654-662.
 - [22] Mankins WL. *Recovery, Recrystallization, and Grain-Growth Structures*. ASM International; 2004. p. 207-214.
 - [23] Sauvage X, Bobruk EV, Murashkin MY, Nasedkina Y, Enikeev NA, Valiev RZ. Optimization of electrical conductivity and strength combination by structure design at the nanoscale in Al-Mg-Si alloys. *Acta Materialia*. 2015; 98: 355-366.
 - [24] Tajally M, Huda Z, Masjuki HH. A comparative analysis of tensile and impact-toughness behavior of cold-worked and annealed 7075 aluminum alloy. *International Journal of Impact Engineering*. 2010; 37(4): 425-432.
 - [25] Ghosh M, Miroux A, Kestens LAI. Correlating r-value and through thickness texture in Al-Mg-Si alloy sheets. *Journal of Alloys and Compounds*. 2015; 619: 585-591.
 - [26] Hort N, Wiese B, Dieringa H, Kainer KU. Protecting molten magnesium and its alloys. *Metallurgia Italiana*. 2016; 6: 105-108.
 - [27] Xu DK, Rometsch PA, Birbilis N. Improved solution treatment for an as-rolled Al-Zn-Mg-Cu alloy. Part II. Microstructure and mechanical properties. *Materials Science and Engineering: A*. 2012; 534: 244-252.
 - [28] Peng G, Chen K, Chen S, Fang H. Evolution of the second phase particles during the heating-up process of solution treatment of Al-Zn-Mg-Cu alloy. *Materials Science and Engineering A*. 2015; 641: 237-241.
 - [29] Shu WX, Hou LG, Liu JC, Zhang C, Zhang F, Liu JT, et al. Solidification paths and phase components at high temperatures of high-Zn Al-Zn-Mg-Cu alloys with different Mg and Cu contents. *Metallurgical and Materials Transactions A*. 2015; 46: 5375-5392.
 - [30] Li Y, Deng Y, Fan S, Guo X, Jiang K, Zhang Z, et al. An in-situ study on the dissolution of intermetallic compounds in the Al-Zn-Mg-Cu alloy. *Journal of Alloys and Compounds*. 2020; 829: 154612.
 - [31] Goloborodko A, Ito T, Yun X, Motohashi Y, Itoh G. Friction stir welding of a commercial 7075-T6 aluminum alloy:

- Grain refinement, thermal stability and tensile properties. *Materials Transactions*. 2004; 45(8): 2503-2508.
- [32] Callegari-Jacques SD. *Bioestatística: Princípios e Aplicações*. Porto Alegre, Brasil: Artimed; 2006.
- [33] Wang JY. Effect of solute content and temperature on the deformation mechanisms and critical resolved shear stress in Mg-Al and Mg-Zn alloys. *Acta Materialia*. 2019; 170: 155-165.
- [34] Santos IC, Asakawa GN, Brandao LPM. Correlation global parameter between r_m and formability. *Tecnologia em Metalurgia Materiais e Mineração*. 2016; 13(2): 157-160.
- [35] Ray RK, Jonas JJ, Hook RE. Cold rolling and annealing textures in low carbon and extra low carbon steels. *International Materials Reviews*. 1994; 39(4): 129-172.
- [36] Prangnell PB, Bate PS, Humphreys FJ. Fundamentals of deformation and annealing-proceedings of the international symposium held to coincide with the retirement of professor. *International Symposium on Fundamentals of Deformation and Annealing*. Manchester, UK; 2007. p. 550.
- [37] Sorger GL. Non-destructive microstructural analysis by electrical conductivity: Comparison with hardness measurements in different materials. *Journal of Materials Science & Technology*. 2019; 35(3): 360-368.
- [38] Cai SL, Wan JC, Hao YJ, Koch CC. Dual gradient microstructure to simultaneously improve strength and electrical conductivity of aluminum wire. *Materials Science and Engineering: A*. 2020; 783: 139308.
- [39] Karabay S, Feyzullahoğlu E. Determination of early failure sources and mechanisms for Al 99.7% and Al-Mg-Si alloy bare conductors used in aerial transmission lines. *Engineering Failure Analysis*. 2014; 38: 1-15.
- [40] Karabay S, Güven EA, Ertürk AT. Enhancement on Al-Mg-Si alloys against failure due to lightning arc occurred in energy transmission lines. *Engineering Failure Analysis*. 2013; 31: 153-160.
- [41] Karabay S. Influence of AlB_2 compound on elimination of incoherent precipitation in artificial aging of wires drawn from redraw rod extruded from billets cast of alloy AA-6101 by vertical direct chill casting. *Materials & Design*. 2008; 29(7): 1364-1375.
- [42] Karabay S. Modification of AA-6201 alloy for manufacturing of high conductivity and extra high conductivity wires with property of high tensile stress after artificial aging heat treatment for all-aluminium alloy conductors. *Materials & Design*. 2006; 27(10): 821-832.
- [43] Karabay S, Yilmaz M, Zeren M. Investigation of extrusion ratio effect on mechanical behaviour of extruded alloy AA-6101 from the billets homogenised-rapid quenched and as-cast conditions. *Journal of Materials Processing Technology*. 2005; 160(2): 138-147.
- [44] Karabay S, Tayşı Y. Improving short-circuit current capacity, resistance, and breaking load of OPGW constructions by modifying aluminium alloy with AlB_2 . *Materials and Manufacturing Processes*. 2004; 19(6): 1157-1169.